

Charge: A Comprehensive Novel View Synthesis Benchmark and Dataset to Bind Them All

Michal Nazarczuk Thomas Tanay Arthur Moreau Zhensong Zhang Eduardo Pérez-Pellitero
Huawei Noah's Ark Lab
London, UK

[michal.nazarczuk1, thomas.tanay, arthur.moreau3, zhangzhensong, e.perez.pellitero]@huawei.com



Figure 1. Charge is a new dataset that binds diverse scenarios related to static and dynamic novel view synthesis, characterised by high-quality renderings and rich annotations. The example includes left-to-right: object segmentation, normals, RGB, depth, and optical flow.

Abstract

This paper presents a new dataset for Novel View Synthesis, generated from a high-quality, animated film with stunning realism and intricate detail. Our dataset captures a variety of dynamic scenes, complete with detailed textures, lighting, and motion, making it ideal for training and evaluating cutting-edge 4D scene reconstruction and novel view generation models. In addition to high-fidelity RGB images, we provide multiple complementary modalities, including depth, surface normals, object segmentation and optical flow, enabling a deeper understanding of scene geometry and motion. The dataset is organised into three distinct benchmarking scenarios: a dense multi-view camera setup, a sparse camera arrangement, and monocular video sequences, enabling a wide range of experimentation and comparison across varying levels of data sparsity. With its combination of visual richness, high-quality annotations, and diverse experimental setups, this dataset offers a unique resource for pushing the boundaries of view synthesis and 3D vision.

1. Introduction

Access and availability of high-quality, large-scale datasets for training and evaluation of algorithms is one of the main

engines for progress and innovation in computer vision. With the advent of the internet, an abundance of readily available images unlocked unprecedented developments in many tasks, *e.g.* image classification, or low-level vision, especially when leveraging forms of self-supervision that alleviate the need for costly manual data annotation.

Recently, NeRF [26] or 3DGS [15] reconstruct the scene by fitting a representation supervised via differentiable rendering and photometric loss on a set of posed 2D images. This coupled with *off-the-shelf* Structure-from-Motion (SfM) camera pose estimators such as COLMAP [33], can reconstruct 3D from a handful of 2D images. Differentiable rendering has received a significant number of follow-up works, *e.g.* dense, sparse, varying appearance. Most of these assume static scenes and fixed radiance fields.

A new generation of feed-forward foundational models, pioneered by VGGT [38], has emerged as a unified architecture capable of predicting multiple 3D representations (camera poses, depth, point clouds, 3D Gaussians [12]) in a single forward pass. These models promise efficient inference and broad generalisation across diverse scenarios without per-scene optimisation. Due to lack of better options, these foundational models have been evaluated almost exclusively on unimodal benchmarks (*i.e.* separately for camera pose estimation, depth, NVS), leaving a gap in the evaluation to further understand and assess the relation-

Table 1. A summary and comparison of datasets used in dynamic novel view synthesis. The top section includes datasets used for multi-view evaluation whereas the middle section focuses on monocular evaluation data. [†] - 2 camera rig with alternating frames assigned to training and test trajectory.

Dataset	Dense	Sparse	Mono	Depth	FPS	# Seq	# Train cams	# Test cams	# Frames
Neural 3D Video [19]	✓	✗	✗	✗	30	6	20	1	56 700
Technicolor [32]	✓	✗	✗	✗	30	5	15	1	25 696
Google Immersive [3]	✓	✗	✗	✗	30	7	45	1	157 320
Nvidia Dynamic [44]	✓	✗	✗	✓	60	8	1	11	2 304
D-NeRF [30]	✗	✗	✓	✗	60	8	1	1	1 410
Nerfies [28]	✗	✗	✓	✗	5	4	1 [†]	1 [†]	1 680
HyperNeRF [29]	✗	✗	✓	✗	15	17	1 [†]	1 [†]	2 152
DyCheck [7]	✗	✗	✓	✓	60	7+7	1	2/0	8 746
Ours	✓	✓	✓	✓	96	8	25+9+4	16+10+16	185 600

ships between the output modalities, and more generally between geometry and appearance.

Extending static to dynamic scene reconstruction is also one of the most promising directions of research, either as a feed-forward or optimisation methodologies. There has been recent interest in addressing this problem, with early paradigms extending NeRF [29, 30] or 3DGS [22, 42, 48] with temporal deformation. Capturing dynamic scenes is inherently difficult. As opposed to static scenes, camera pose estimation on dynamic scenes is a challenging and largely unsolved problem, *i.e.* movement in the scene can introduce matching errors that then degrade the estimated poses. Furthermore, due to low image sampling rates (*e.g.* 24 fps), *soft* or inaccurate camera synchronisation can in turn impact the camera pose and reconstruction accuracy. In practice, complex, hardware-synchronised multi-camera systems are needed to obtain multiple views of the scene [20, 25]. Such rigs restrict the scene diversity due to the limitations on physical spaces where they can be deployed (*i.e.* indoors, volumetric studios), and ultimately can not be moved within the scene (in part due to weight, fragility and build, but also because of potential problems with camera calibration). The need for testing views results in a reduction of the number of training views available, a trade-off that often result in poor camera sampling for evaluation. For approaches where separated, non-synchronised cameras are used for the testing views [7], problems can arise in the camera calibration in dynamic scenes. This, coupled with the lack of precise temporal frame alignment, degrades the ability to accurately evaluate the performance of 4D reconstruction methods.

Given the technical limitations to capture 4D posed data, we find inspiration in the *MPI Sintel* dataset [4]. In our work, we present a novel high-resolution, dynamic dataset for unified 3D evaluation with rich modalities (RGB, depth, normals, segmentation), and overcomplete training and testing camera coverage that addresses open challenges of 3D reconstruction. The dataset is arranged for different

static and dynamic reconstruction setups: dense, sparse, and monocular inputs, and supports full evaluation of current and next generation foundational models (camera pose, depth, NVS). We show a visualisation of the modalities in Fig. 1, and an overview of the dataset composition in Fig. 2. This dataset is generated from the high-quality animated movie *Charge* [8] including rich scene compositions and a variety of content. The synthetic nature of the dataset allows us to introduce a large-scale dataset and benchmark not viable to be collected in the real world due to capture cost, physical limitations, and ultimately accurate pose estimation. We summarise our contributions as follows:

1. We introduce a new synthetic dataset - *Charge* - for next generation models benchmarking, including dynamic NVS, 3D foundational models. It is characterised by high visual quality, it outscapes other available datasets in the number of images, and it provides rich annotations offering a variety of additional modalities.
2. We unify all relevant reconstruction setups - Static, Dynamic, Dense, Sparse, Mono, and provide benchmarking for all of them.
3. We perform an extensive evaluation of state-of-the-art reconstruction methods and analyse the results emphasising the importance of the benchmark we propose.

2. Related Work

Advances in novel view synthesis include the introduction of two seminal reconstruction paradigms, namely Neural Radiance Fields [26] and 3D Gaussian Splatting [15]. These developments in static scene reconstruction were quickly followed by several works on dynamic content.

Dynamic Reconstruction: NeRF-based methods for video reconstruction include D-NeRF [30], StreamRF [18], HexPlane [5], K-Planes [6], Tensor4D [34], MixVoxels [37]. Representative monocular approaches include NSFF [21], Nerfies [28], HyperNeRF [29], DyCheck [7]. Similarly, Gaussian Splatting enabled reconstruction of multi-view videos, *e.g.* GaussianFlow [23], 4DGS [42], STG [22], Mo-



Figure 2. An overview of the Charge dataset. The left side presents a selection of frames from all the animations. On the right side, a 3 setups included in the dataset are presented: Dense, Sparse, and Mono. Cameras allocation and sample movement path for monocular trajectory are overlayed on the section of the point cloud corresponding to scene 040_0040.

tionGS [48], SWinGS [35], Ex4DGS [16]. The most recent advances in Gaussian Splatting include monocular video reconstructions by works such as Deformable 3D Gaussians [43], SC-GS [11], or MoSca [17].

Foundational models: The recent advances in feed-forward geometry estimation emphasise the need for unified benchmarking. VGGT [38] introduced a transformer architecture for multiple 3D tasks, including camera parameter estimation, depth estimation, point cloud reconstruction, 3D tracking. This, along with follow-up works [14, 39, 40] established a group of foundational 3D models trained in a supervised manner on large-scale data. Several works offer pipelines that predict gaussians from a set of unposed views [9, 10, 47]. AnySplat [12] and WorldMirror [24] build upon VGGT to enable gaussian splat prediction for NVS.

Datasets: Current evaluation of dynamic NVS is based on a handful of datasets summarised in Table 1. This includes real-world data. Neural 3D Video [19] introduces indoor cooking scenes captured with a static rig. Technicolor [32] provides several scenes captured with a rig of 4x4 cameras. The shortcoming of the two datasets is the reduced amount of dynamic content (*e.g.* cooking occupies only a small region of the videos), and relatively slow motions. Additionally, those datasets evaluate the performance only on 1 camera selected from the rig. Google Immersive [3] provides videos captured with a spherical rig of outward-facing cameras and suffers from heavy fish-eye distortions and very

low overlap between views. DiVa-360 [25] captures a set of objects and hand-object interactions. Stereo4D [13] offers a dataset extracted from stereoscopic fisheye videos. DynPose [31] filters and annotates internet videos with camera poses. Monocular datasets include *e.g.* Nvidia Dynamic Scene [44] which introduces sequences captured by a rig of 12 cameras subsampling alternating views to create a monocular trajectory. Nerfies [28] and HyperNeRF [29] capture action with two cameras and alternate their frames in the input and test sequences. They suffer from highly unrealistic motion due to teleporting cameras creating thus a pseudo-multi-view capture. This is characterised as a high effective multi-view factor in DyCheck [7], which introduces a new monocular capture with 2 static cameras for evaluation. However, it suffers from an imperfect set of camera poses. A better set of camera poses can be seen in DTU [1] captured with a camera mounted on a robotic arm. It is broadly used in novel view synthesis evaluation in dense and sparse setups. However, it provides only static scenes. Similarly, Sparse Neural Rendering Dataset [27] provides a DTU-like setup but in a synthetic version, and thus is also static and present a single object per scene. D-NeRF [30] is a synthetic dataset of dynamic content. It captures lower-quality subject assets on a white background. Further, it creates a monocular input sequence by sampling consecutive cameras (suffering from teleporting-related issues). In contrast, Charge provides high-quality renderings

Table 2. Percentage of dynamic content in various datasets.

Data	Charge	DyCheck	Neural 3D	Technicolor
Dynamic	25.1 %	12.6 %	10.9 %	9.7 %

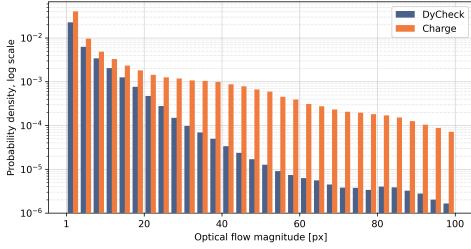


Figure 3. Optical flow histogram for DyCheck and Charge.

of rich sequences with carefully designed setups for dense and sparse multi-view, and monocular captures.

In Table 2, we show a breakdown of dynamic content in current datasets by presenting a percentage of pixels occupied by dynamic objects. Notably, frames in Charge are occupied on average by twice the amount of dynamic parts than the closest competitor. Similarly, in Figure 3 we show histograms of optical flow magnitude for our Charge in comparison to DyCheck [7] for their respective dynamic regions. Charge has higher density of dynamic pixels, and has better coverage across the diverse magnitudes, with special advantages on large motions.

3. The Charge Dataset

In this work we introduce a new dataset for evaluating new generation models, including but not limited to dynamic NVS and 3D foundation models. In pursue of high-quality data, we explored animated movies created in the rendering software Blender [2]. Specifically, we focus on Charge, a short movie set in a dystopian world, created to showcase Blender’s photorealistic rendering capabilities.

3.1. Dataset Creation

We utilise production shots from the Charge movie to create our dataset. For each such scene a composition with animation, lighting, and a library of items is available. We processed all 8 available scenes for Charge of which examples can be seen in Figure 2 (left). For every scene, we manually picked places for cameras for the best capture and visibility of the scene after spanning the whole rig. Additionally, we removed the original rendering pipeline due to postprocessing effects that may degrade the 3D consistency of the capture. Instead, we replace the rendering pipeline with direct rendering from the camera, and we add rendering of additional modalities (such as depth, or normals).

3.2. Camera Setups

The Charge dataset provides the unique benchmarking feature of having various camera setups corresponding to com-

monly tackled novel view synthesis problems within the exact same scenes, namely: Dense, Sparse, and Mono. Commonly used camera setups include the use of coplanar capture or dome capture. Inspired by that, we decided to place the cameras on the section of the sphere, such that scenes are mostly forward-facing (similar to most real-world captures), yet offer the benefits of changing perspective. To this end, we manually adjust the position of the rig and the radius of the aforementioned sphere for each scene.

Dense setup consists of 25 training cameras and 16 testing cameras (see Fig. 2 top right). This offers a setup similar to Neural 3D Video [19] or Technicolor [32]. Those works, limited by the constraints of the real world (high capture cost), offer only one camera for testing. We provide 16 testing cameras allowing for a more thorough evaluation.

Sparse setup follows a common practise in literature (e.g. pixelNeRF [45]) and we provide training scenarios including 3, 6, or 9 training cameras, accompanied by 10 testing views (see Fig. 2 middle right). Note that the sparse setup covers the scenes from a different perspective instead of simply subsampling the training cameras. This increases the diversity of our dataset and opens up new areas of research and exploration when performing distant novel view synthesis, i.e. with an emphasis on view extrapolation as opposed to interpolation.

Mono setup introduces 4 different trajectories of the monocular camera. We aim to reproduce in this setup camera motions that are viable with a handheld device. As characterised by DyCheck, a monocular capture should not exhibit a high effective multiview factor (e.g. teleporting or extremely fast camera). To this end, based on empirical experimentation with the use of a phone camera and a target captured from around 1 – 2m, we estimate that the reasonable velocity of a capture device lies around the range of 15 – 50 cm/s. Therefore, we introduce *Fast* and *Slow* monocular trajectories corresponding roughly to the upper and lower bounds of the measured values. Similarly, we propose that the capture may deliberately try to cover a wider perspective or be less regularised. Hence, we suggest two qualities of the camera trajectory: *Spline* - constrained to a spline curve spanning the majority of corresponding training camera positions, and *Random Walk* - randomly generated direction for every time step with a smoothing factor. This results in the following training scenarios: *SplineFast*, *SplineSlow*, *RandomWalkFast*, *RandomWalkSlow*. Further, monocular reconstruction encompasses many downstream goals, such as stabilisation, or spatial video (stereo pair synthesis). Thus, we propose to test each of these trajectories with 4 static cameras chosen from the set of Dense testing cameras (allowing for direct comparison), and 4 cameras defined relative to the training one (different baselines, and a camera orbiting around).

Table 3. Quantitative evaluation results of Charge dataset - Dense and Mono setups, -D denotes metrics on dynamic-only areas, -S static only and FOV_O quantifies the field-of-view overlap between testing and training views (*i.e.* harder when lower). Best performer.

Method	PNSR	PNSR-D	PNSR-S	SSIM	SSIM-D	LPIPS	LPIPS-D	FOV_O
Dense								
4DGS [42]	28.94	26.84	<u>31.85</u>	0.881	0.848	0.231	0.307	0.70
STG [22]	29.29	28.15	31.33	0.886	<u>0.866</u>	0.193	<u>0.263</u>	0.70
Ex4DGS [16]	<u>29.75</u>	<u>28.57</u>	31.57	<u>0.893</u>	0.863	<u>0.187</u>	0.264	0.70
Mono - Spline Fast								
4DGS [42]	24.85	22.69	<u>27.25</u>	0.840	0.794	0.264	0.352	0.42
D-3DGS [43]	<u>24.88</u>	22.91	<u>27.24</u>	<u>0.869</u>	0.807	<u>0.201</u>	0.295	0.42
SC-GS [11]	23.97	<u>23.57</u>	25.89	0.847	0.798	0.217	<u>0.291</u>	0.42
MoSca [17]	23.39	22.84	24.10	0.853	<u>0.817</u>	0.255	0.320	0.42
Mono - Spline Slow								
4DGS [42]	<u>24.18</u>	21.95	<u>26.65</u>	0.834	0.787	0.266	0.360	0.41
D-3DGS [43]	<u>24.18</u>	22.53	26.15	0.858	0.794	<u>0.203</u>	<u>0.290</u>	0.41
SC-GS [11]	23.29	22.54	25.15	0.843	0.786	0.225	0.304	0.41
MoSca [17]	23.45	<u>22.83</u>	24.63	0.856	<u>0.815</u>	0.244	0.323	0.41
Mono - Random Walk Fast								
4DGS [42]	<u>24.78</u>	22.79	<u>26.81</u>	0.835	0.790	0.267	0.359	0.41
D-3DGS [43]	24.34	22.55	26.24	0.852	0.789	<u>0.217</u>	<u>0.309</u>	0.41
SC-GS [11]	22.90	<u>23.04</u>	24.22	0.822	0.775	<u>0.243</u>	0.314	0.41
MoSca [17]	23.82	22.77	25.09	<u>0.857</u>	<u>0.817</u>	0.251	0.325	0.41
Mono - Random Walk Slow								
4DGS [42]	23.38	21.68	<u>25.64</u>	0.818	0.771	0.277	0.370	0.38
D-3DGS [43]	22.85	21.61	24.76	0.829	0.762	<u>0.227</u>	0.318	0.38
SC-GS [11]	21.86	21.73	23.51	0.811	0.762	0.244	0.318	0.38
MoSca [17]	<u>24.29</u>	<u>23.61</u>	25.23	<u>0.871</u>	<u>0.829</u>	0.229	<u>0.306</u>	0.38

3.3. Data Qualities

As visible on the left-hand side of Figure 2, Charge introduces a large diversity of scenes posing challenging and interesting problems for 3D reconstruction methods. Examples include a scene with large open bounds and a smaller dynamic subject (020.0020), with a large amount of movement (040.0040), with a large area of dynamic content (070.0123), or highly non-rigid elements (050.0130).

With the development of 3DGS, the high-resolution evaluation became viable and is arguably preferable. Thus, we render our dataset in a resolution of **2048×858**. Further, we provide a high-speed capture in **96 fps**. Additionally, thanks to the synthetic nature of our data, we are able to provide highly precise camera poses in contrast to real-world captures that rely on estimations. Finally, along with *RGB images*, we supply **metric depth, optical flow, normals, UV maps, object segmentation, and dynamic content masks**.

In total, Charge offers **8** diverse scenes, each rendered with **25+16** dense setup cameras, **9+10** sparse setup cameras, and **4+16** monocular setup cameras. This accounts for a total of **185 600** frames available, providing a larger scale of data than any other existing datasets (see Tab. 1).

4. Benchmark

We evaluate the Charge dataset with a selection of methods representing the state-of-the-art in multi-view and monocular Gaussian Splatting reconstruction. We report a large

selection of metrics, introducing a measure of difficulty for each task, and analyse the results, focusing on challenges available in our dataset that emphasise problems that are difficult for current methods to deal with. We include dynamic evaluation on scene-specific methods and a static evaluation on next generation foundational models.

4.1. Dynamic Benchmark

We provide evaluation for all 3 setups in our dataset, namely Dense, Sparse, and Mono. Therefore, we use 4D Gaussian Splatting [42] to train all sequences in all setups, as it is a method suitable for both multi- and single-view reconstruction. Further, we use Spacetime Gaussians [22] and Ex4DGS [16] to evaluate Dense and Sparse scenarios. Finally, in a monocular setting, we add 3 dedicated methods, Deformable 3D Gaussians [43], SC-GS [11], and MoSca [17]. All methods were trained on full-length sequences and evaluated in full resolution of data in Charge.

Metrics In our evaluation, we report commonly used metrics, such as PSNR, SSIM [41], and LPIPS [46]. Further, for PSNR on dynamic benchmark, we include the metric calculated within the mask of dynamic and static content (PSNR-D and PSNR-S, respectively). Similarly, for SSIM and LPIPS we report a version of these metrics calculated for dynamic content based on a tight bounding box of the dynamic mask (SSIM-D, LPIPS-D).

Additionally, we propose to quantify the difficulty of each task. To this end, we suggest calculating a param-

Table 4. Quantitative evaluation results of Charge dataset - Sparse setup, -D denotes metrics on dynamic-only areas, -S static only and FOV_O quantifies the field-of-view overlap between testing and training views (*i.e.* harder when lower). Best performer.

Method	Views	PNSR	PNSR-D	PNSR-S	SSIM	SSIM-D	LPIPS	LPIPS-D	FOV_O
Sparse									
4DGS [42]	3	19.71	20.71	20.28	0.776	0.740	0.358	0.416	0.54
STG [22]		18.80	20.15	19.04	0.753	0.721	0.371	0.418	0.54
Ex4DGS [16]		19.53	20.34	20.05	0.759	0.717	<u>0.350</u>	<u>0.400</u>	0.54
4DGS [42]	6	23.93	24.89	24.29	0.840	0.810	0.277	0.338	0.62
STG [22]		22.39	23.61	22.57	0.820	0.790	0.295	0.361	0.62
Ex4DGS [16]		22.07	23.30	22.31	0.813	0.781	0.299	0.348	0.62
4DGS [42]	9	26.67	26.51	27.45	0.874	0.840	0.226	0.301	0.64
STG [22]		24.52	24.96	25.03	0.850	0.815	0.260	0.347	0.64
Ex4DGS [16]		24.50	26.26	24.73	0.859	0.829	<u>0.225</u>	<u>0.282</u>	0.64



Figure 4. Example results of rendering in Charge dataset evaluation - Dense setup. Best viewed zoomed in.

ter indicating an overlap between the field of views of the testing camera with respect to training cameras. To this end, for each testing view, we reproject the image plane into all training views obtaining coverage masks - $\{m_i\}$ (effectively saying which area of the testing view is visible from the given training view). Further, we sum up all such masks and normalise them by the number of pixels in training views $n_{train} \cdot HW$, obtaining a weighted covisibility proxy (where pixels seen by more training views have a value closer to 1). Therefore, averaging for n_{test} test views, the field of view overlap is expressed as:

$$FOV_O = \frac{1}{n_{test}} \left(\frac{\sum_{n_{train}} m_i}{n_{train} \cdot HW} \right) \quad (1)$$

Finally, we average the value for all the test views to obtain an indication of task difficulty. A more detailed analysis, along with the breakdown of the metrics, including separation per scene is available in the Supplementary Material.

Dense The results of the experiments on the Dense setup of the Charge dataset are presented in Table 3 (top rows). Additionally, selected qualitative samples can be seen in

Figure 4. We can observe PSNR results of 28.94, 29.29, and 29.75. This indicates that Charge poses a good challenge for current state-of-the-art methods. In Fig. 4 (left side) we can see that all methods struggle with reconstructing a splash of paint which leads us to believe that even in the dense multi-view camera setup, the reconstruction of the dynamics of a highly non-rigid object is yet to be explored in depth. Further, in Fig. 4, right, we note that our dataset provides a good way of evaluating the effect of the length of the sequence on the reconstruction (with sequences ranging from 93 to 653 frames). The given example shows that 4DGS struggles with reconstructing a long-range sequence with a large amount of movement. Notably, however, we do not notice a decrease in the performance with the consecutive frames but rather a consistently lower quality of the reconstruction. Finally, unsurprisingly, we can observe the gap between the reconstruction of dynamic and static regions which is reflected in the presented results. This leads us to believe that data like Charge with a large amount of dynamic content is crucial for an insightful evaluation.

Sparse In Table 4 we present the results of the evaluation on the Sparse setup of the Charge dataset. Note that as indicated in Figure 2 (right), the sparse camera setup does not overlap with the dense one. Therefore, the corresponding numerical values should not be directly compared. However, based on the values of the field of view overlap, we notice that sparse rendering is significantly harder than dense reconstruction. Additionally, we note that the difficulty increase from 6 to 3 training views is higher than from 9 to 6 training views. An example selection of scenes trained and rendered in all scenarios is shown in Figure 5. We can observe that in the lower camera regime, 4DGS and Ex4DGS perform slightly better than STG, indicating that the selection of the best method for the task is configuration-dependent. Further, we can clearly observe, both visually, and in the presented metrics, a drastic difference in performance with respect to the number of training cameras. In Figure 5 we can see that even in 9-views case, the renderings exhibit a lack of fine details (*e.g.* hands in the example). Further, with 6 training views, we notice an increasing num-



Figure 5. Example results of rendering in Charge dataset evaluation - Sparse setup, scene 050_0160. Best viewed zoomed in.

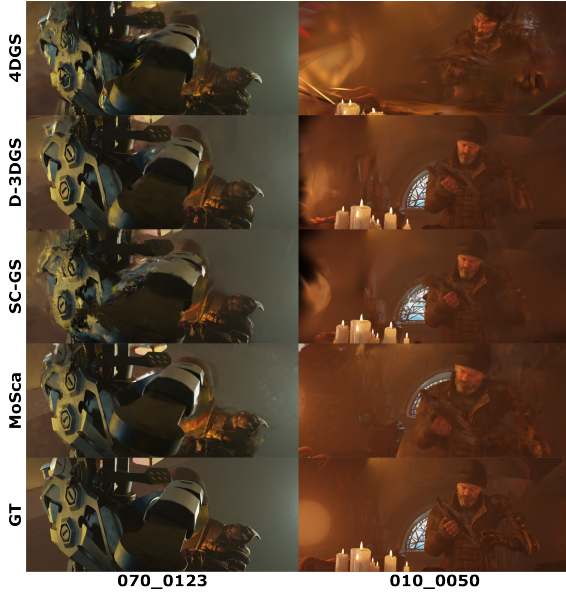


Figure 6. Example results of rendering in Charge dataset evaluation - Mono setup. Best viewed zoomed in.

ber of background missing or incorrect gaussian. Finally, 3 views present a very hard case for the benchmarked methods, leading to very artefact-filled renders. Interestingly, the differences in the reconstruction of dynamic and static content are not as prominent in the Sparse setup. We believe that the decrease in the overlap between cameras leads to higher uncertainties, especially in disoccluded areas, as well as edge areas, seen by a very low number of cameras.

Mono We propose 4 configurations for evaluating monocular trajectories and provide evaluation separated as such, namely *Spline Fast*, *Spline Slow*, *Random Walk Fast*, *Random Walk Slow*. The results from all configurations are presented in Table 3 (bottom rows). A selection of qualitative results for the Mono setup is shown in Fig. 6. This setup is evaluated based on 8 cameras - 4 cameras correspond to central testing cameras from the Dense setup, and 4 further cameras are moving together with the training one (3 represent different baselines in the task of creating stereo pairs,

and 1 camera is orbiting around the training one).

Unsurprisingly, we can notice a decrease in the field of view overlap (increase in difficulty) for this task when compared to the dense setup. We see slight differences between the configurations of the Mono setup, indicating structured (spline covering the area better) and faster (more area covered) motion to be easier to reconstruct.

We notice a similar performance of 4DGS and D-3DGS, and lower for SC-GS. Surprisingly, MoSca (best on DyCheck[7]), performs the best only in the structural metric, being lower on PSNR. This may be caused by evaluation on our dataset with a large amount of motion. MoSca heavily relies on trajectory estimation in a preprocessing step, which seems to be harder on Charge due to the larger range of motion and objects moving into the camera view. Additionally, MoSca optimises camera poses during training, and relies on test time optimisation to update test poses, introducing uncertainty with respect to underlying reconstruction. This emphasises the need for Charge benchmark allowing evaluation with perfect ground-truth cameras. In Fig. 6 we notice that when reconstructing a scene with a large amount of dynamic content close to the camera (e.g. 070_0123), the methods struggle with the reconstruction of such regions. Similarly, as seen in 010_0050, we notice how monocular reconstruction is affected by a lack of coverage outside the field of view causing dark areas near the edges.

4.2. Static Benchmark

In addition, we subselect a set of frames from each scene and propose a static benchmark to evaluate foundational models which currently focus on static scenes only. To this end, we use our **Sparse** and **Dense** setup and evaluate camera pose estimation, depth estimation, and novel view synthesis. We evaluate VGGT [38] and π^3 [40] that do not predict the appearance of the scene, as well as AnySplat [12] and WorldMirror [24] that produce Gaussian splats. We present all results in Table 5.

Camera pose estimation We report AUC at angular thresholds of 5° , 15° , and 30° . AUC is the area under the accuracy-threshold curve of the minimum values between

Table 5. A static benchmark of next generation foundational models on Charge, including camera pose estimation, depth estimation and novel view synthesis, [†] denotes target views used for camera alignment. Best performer.

Method	Camera pose			Depth		NVS			NVS [†]		
	AUC@5 [†]	AUC@15 [†]	AUC@30 [†]	AbsRel [↓]	$\delta < 1.25^{\uparrow}$	PSNR [†]	SSIM [†]	LPIPS [↓]	PSNR [†]	SSIM [†]	LPIPS [↓]
Sparse-3	VGGT [38]	<u>0.3581</u>	<u>0.7599</u>	<u>0.8809</u>	0.1039	0.8669	-	-	-	-	-
	π^3 [40]	0.1900	0.6376	0.8127	<u>0.1014</u>	0.8895	-	-	-	-	-
	AnySplat [12]	0.2827	0.7394	0.8708	0.2101	0.7557	12.15	0.6723	0.6080	13.34	0.7065
	WorldMirror [24]	0.3547	0.7148	0.8555	0.2003	0.7565	<u>17.54</u>	<u>0.7318</u>	<u>0.5648</u>	<u>20.94</u>	<u>0.7841</u>
Sparse-6	VGGT [38]	0.5009	0.8086	0.9046	0.0959	0.8679	-	-	-	-	-
	π^3 [40]	0.2844	0.7118	0.8565	<u>0.0896</u>	<u>0.9191</u>	-	-	-	-	-
	AnySplat [12]	0.3751	0.7733	0.8871	0.1721	0.7970	13.27	0.6972	0.5822	15.95	0.7359
	WorldMirror [24]	<u>0.5049</u>	<u>0.8164</u>	<u>0.9087</u>	0.1601	0.7873	<u>18.97</u>	<u>0.7560</u>	<u>0.5472</u>	<u>21.86</u>	<u>0.7958</u>
Sparse-9	VGGT [38]	<u>0.5188</u>	<u>0.8161</u>	<u>0.9087</u>	0.0992	0.8681	-	-	-	-	-
	π^3 [40]	0.2886	0.7183	0.8596	<u>0.0909</u>	<u>0.9133</u>	-	-	-	-	-
	AnySplat [12]	0.3731	0.7667	0.8837	0.1981	0.7727	16.30	0.7345	0.5541	19.52	0.7755
	WorldMirror [24]	0.4919	0.8066	0.9032	0.1781	0.7904	<u>19.57</u>	<u>0.7671</u>	<u>0.5436</u>	<u>22.84</u>	<u>0.8122</u>
Dense	VGGT [38]	<u>0.5149</u>	0.8011	0.8996	<u>0.1085</u>	0.8499	-	-	-	-	-
	π^3 [40]	0.4071	0.7634	0.8807	0.1344	0.8893	-	-	-	-	-
	AnySplat [12]	0.3359	0.7524	0.8767	0.2248	0.7595	18.74	0.7440	0.5533	23.12	0.7943
	WorldMirror [24]	0.5126	<u>0.8205</u>	<u>0.9093</u>	0.1811	0.7632	<u>20.10</u>	<u>0.7666</u>	<u>0.5475</u>	<u>24.44</u>	<u>0.8192</u>

Relative Rotation Accuracy and Relative Translation Accuracy across varying thresholds. We note a close performance between VGGT and WorldMirror which share a VGGT backbone. Notably AnySplat even though initialised from VGGT performs worse indicating a degradation of camera head performance in the model. π^3 is noticeably worse in lower threshold metrics.

Depth estimation We report Absolute Relative Error and threshold accuracy of 25%. In this task, π^3 is the best performer, in contrast to camera pose evaluation. VGGT’s performance is a close second, whereas the methods that output Gaussian splats decrease the depth estimation performance in the course of photometric supervision.

Novel View Synthesis We report PSNR, SSIM, LPIPS, a commonly used metrics in novel view synthesis. The benchmark methods provide results in an arbitrary scale. Therefore, we distinguish two testing protocols in this task present in literature. In first, we align the target cameras to the models prediction by fitting a ground truth to predicted pose transformation on the source views (Umeyama [36]). In the second, we follow AnySplat protocol, *i.e.* we run the model again on the set of both source and target views to then use the predicted target cameras to render Gaussians predicted from source views. In this experiment we observe WorldMirror outperforming AnySplat. This correlates with camera pose estimation results, and in qualitative examples (Supp. Mat.), we observe misalignment between target and ground truth images. Further, the Umeyama alignment performs significantly worse than using target views for alignment. Given the perfect ground truth camera pose, this emphasises a pose-shape ambiguity in the predicted geometries. Importantly, when including photometric consistency in the pipeline, the methods preserve the relative ranking across all tasks in contrast to directly supervised ones

(VGGT and π^3). This suggest that the coupling of NVS and geometry tasks may have a negative effect on the performance of the current models. Notably, this analysis can only be performed in a dataset with perfect ground truth for both geometry and appearance, such as Charge.

5. Conclusions

In this paper, we introduced Charge, a new dataset and benchmark for novel view synthesis. Our dataset was rendered from a professionally created animation movie. This enables us to obtain photorealistic data, with detailed shapes and textures as well as intricate movements and interactions. Charge offers several advantages over real-world datasets: (1) various capture setups for different problems (static, dynamic, dense, sparse, monocular), (2) with high number of testing cameras, and (3) with accurate camera poses, thus increasing the reliability of the evaluation. (4) Charge contains more motion than any other dataset to date, and (5) this motion is more diverse, *i.e.* ranging from small to large displacements. (6) Charge includes rich annotations, including 6 data modalities, encouraging the development of new methods and novel evaluation paradigms.

We extensively tested the performance of SoTA GS-based and 3D foundational models on this data. We provided a thorough analysis of the selected methods in all proposed setups. Our evaluation emphasises the shortcomings of current approaches by showing areas that need improvement, based on several aspects and input features, *e.g.* camera speed, trajectory style, static vs dynamic performance. Finally, the performance of the state-of-the-art methods in the Charge benchmark shows that the data we propose is challenging, and that it can be an accelerator in developing and evaluating the next generation NVS approaches.

References

- [1] Henrik Aanæs, Rasmus Ramsbøl Jensen, George Vogiatzis, Engin Tola, and Anders Bjrholm Dahl. Large-Scale Data for Multiple-View Stereopsis. *IJCV*, 120:1–16, 2016. 3
- [2] Blender Online Community. Blender, 2022. accessed on 27th February 2025. 4
- [3] Michael Broxton, John Flynn, Ryan Overbeck, Daniel Erickson, Peter Hedman, Matthew DuVall, Jason Dourgarian, Jay Busch, Matt Whalen, and Paul Debevec. Immersive Light Field Video with a Layered Mesh Representation. *ACM Transactions on Graphics*, 39(4):86:1–86:15, 2020. 2, 3
- [4] Daniel J. Butler, Jonas Wulff, Garrett B. Stanley, and Michael J. Black. A naturalistic open source movie for optical flow evaluation. In *European Conference on Computer Vision (ECCV)*, 2012. 2
- [5] Ang Cao and Justin CV. HexPlane: A Fast Representation for Dynamic Scenes. In *Computer Vision and Pattern Recognition Conference (CVPR)*, 2023. 2
- [6] Sara Fridovich-Keil, Giacomo Meanti, Frederik Rahbæk Warburg, Benjamin Recht, and Angjoo Kanazawa. K-Planes: Explicit Radiance Fields in Space, Time, and Appearance. In *Computer Vision and Pattern Recognition Conference (CVPR)*, 2023. 2
- [7] Hang Gao, Ruilong Li, Shubham Tulsiani, Bryan Russell, and Angjoo Kanazawa. Monocular Dynamic View Synthesis: A Reality Check. In *Conference on Neural Information Processing Systems*, 2022. 2, 3, 4, 7
- [8] Hjalti Hjalmarsson, Andy Goralczyk, Rik Schutte, Francesco Siddi, Ton Roosendaal, Torin Borrowdale, Sander Houtman, Cristo Pruppers, Ian Yeromenko, Pavlo Nivievskyi, Dmytro Kniazhechenko, Beau Gerbrands, Demeter Dzadik, Julien Kaspar, Pablo Fournier, Simon Thommes, Brecht Van Lommel, Sergey Sharybin, Campbell Barton, Dalai Felinto, Julian Eisel, Jacques Lucke, Hans Goudey, Clément Foucault, Bastien Montagne, Sybren Stüvel, Jeroen Bakker, Sebastian Parborg, Anja Vugtst-Verstappen, Pablo Vazquez, Anna Sirota, Arnd Marijnissen, Danny McGrath, Snorri Styrkársson, Styrkár Snorrason, and Carlos Baena. Charge, 2022. Short movie by Blender Studio. <https://studio.blender.org/projects/charge/> accessed on 27th February 2025. 2
- [9] Sunghwan Hong, Jaewoo Jung, Heeseong Shin, Jisang Han, Jiaolong Yang, Chong Luo, and Seungryong Kim. Pf3plat: Pose-free feed-forward 3d gaussian splatting. In *International Conference on Machine Learning (ICML)*, 2025. 3
- [10] Ranran Huang and Krystian Mikolajczyk. No pose at all: Self-supervised pose-free 3d gaussian splatting from sparse views. In *International Conference on Computer Vision (ICCV)*, 2025. 3
- [11] Yi-Hua Huang, Yang-Tian Sun, Ziyi Yang, Xiaoyang Lyu, Yan-Pei Cao, and Xiaojuan Qi. SC-GS: Sparse-Controlled Gaussian Splatting for Editable Dynamic Scenes. In *Computer Vision and Pattern Recognition Conference (CVPR)*, 2023. 3, 5
- [12] Lihan Jiang, Yucheng Mao, Linning Xu, Tao Lu, Kerui Ren, Yichen Jin, Xudong Xu, Mulin Yu, Jiangmiao Pang, Feng Zhao, Dahua Lin, and Bo Dai. AnySplat: Feed-forward 3D Gaussian Splatting from Unconstrained Views. In *SIGGRAPH Asia*, 2025. 1, 3, 7, 8
- [13] Linyi Jin, Richard Tucker, Zhengqi Li, David Fouhey, Noah Snavely, and Aleksander Holynski. Stereo4D: Learning How Things Move in 3D from Internet Stereo Videos. In *Computer Vision and Pattern Recognition Conference (CVPR)*, 2025. 3
- [14] Nikhil Keetha, Norman Müller, Johannes Schönberger, Lorenzo Porzi, Yuchen Zhang, Tobias Fischer, Arno Knapitsch, Duncan Zauss, Ethan Weber, Nelson Antunes, Jonathon Luiten, Manuel Lopez-Antequera, Samuel Rota Bulò, Christian Richardt, Deva Ramanan, Sebastian Scherer, and Peter Kotschieder. MapAnything: Universal feed-forward metric 3D reconstruction. In *arXiv:2509.13414*, 2025. 3
- [15] Bernhard Kerbl, Georgios Kopanas, Thomas Leimkühler, and George Drettakis. 3D Gaussian Splatting for Real-Time Radiance Field Rendering. *ACM Transactions on Graphics*, 42(4), 2023. 1, 2
- [16] Junoh Lee, Changyeon Won, Hyunjun Jung, Inhwon Bae, and Hae-Gon Jeon. Fully Explicit Dynamic Gaussian Splatting. In *Proceedings of the Neural Information Processing Systems*, 2024. 3, 5, 6
- [17] Jiahui Lei, Yijia Weng, Adam Harley, Leonidas Guibas, and Kostas Daniilidis. MoSca: Dynamic gaussian fusion from casual videos via 4D motion scaffolds. In *Computer Vision and Pattern Recognition Conference (CVPR)*, 2025. 3, 5
- [18] Lingzhi Li, Zhen Shen, Zhongshu Wang, Li Shen, and Ping Tan. Streaming Radiance Fields for 3D Video Synthesis. In *Conference on Neural Information Processing Systems*, 2022. 2
- [19] Tianye Li, Mira Slavcheva, Michael Zollhöfer, Simon Green, Christoph Lassner, Changil Kim, Tanner Schmidt, Steven Lovegrove, Michael Goesele, Richard Newcombe, and Zhaoyang Lv. Neural 3D Video Synthesis from Multi-view Video. In *Computer Vision and Pattern Recognition Conference (CVPR)*, 2022. 2, 3, 4
- [20] Tianye Li, Mira Slavcheva, Michael Zollhöfer, Simon Green, Christoph Lassner, Changil Kim, Tanner Schmidt, Steven Lovegrove, Michael Goesele, Richard A. Newcombe, and Zhaoyang Lv. Neural 3d video synthesis from multi-view video. In *Computer Vision and Pattern Recognition Conference (CVPR)*, 2022. 2
- [21] Zhengqi Li, Simon Niklaus, Noah Snavely, and Oliver Wang. Neural Scene Flow Fields for Space-Time View Synthesis of Dynamic Scenes. In *Computer Vision and Pattern Recognition Conference (CVPR)*, 2021. 2
- [22] Zhan Li, Zhang Chen, Zhong Li, and Yi Xu. Spacetime Gaussian Feature Splatting for Real-Time Dynamic View Synthesis. In *Computer Vision and Pattern Recognition Conference (CVPR)*, 2024. 2, 5, 6
- [23] Youtian Lin, Zuozhuo Dai, Siyu Zhu, and Yao Yao. Gaussian-Flow: 4D Reconstruction with Dynamic 3D Gaussian Particle. In *Computer Vision and Pattern Recognition Conference (CVPR)*, 2024. 2
- [24] Yifan Liu, Zhiyuan Min, Zhenwei Wang, Junta Wu, Tengfei Wang, Yixuan Yuan, Yawei Luo, and Chunchao Guo. World-

- Mirror: Universal 3D World Reconstruction with Any-Prior Prompting. *arXiv preprint arXiv:2510.10726*, 2025. 3, 7, 8
- [25] Cheng-You Lu, Peisen Zhou, Angela Xing, Chandradeep Pokhariya, Arnab Dey, Ishaan N Shah, Rugved Mavidipalli, Dylan Hu, Andrew Comport, Kefan Chen, and Srinath Sridhar. Diva-360: The dynamic visual dataset for immersive neural fields. In *Computer Vision and Pattern Recognition Conference (CVPR)*, 2024. 2, 3
- [26] Ben Mildenhall, Pratul P. Srinivasan, Matthew Tancik, Jonathan T. Barron, Ravi Ramamoorthi, and Ren Ng. NeRF: Representing scenes as neural radiance fields for view synthesis. In *European Conference on Computer Vision (ECCV)*, 2020. 1, 2
- [27] Michal Nazarczuk, Thomas Tanay, Sibi Catley-Chandar, Richard Shaw, Radu Timofte, and Eduardo Pérez-Pellitero. AIM 2024 Sparse Neural Rendering Challenge: Dataset and Benchmark. In *European Conference on Computer Vision Workshops (ECCVW)*, 2024. 3
- [28] Keunhong Park, Utkarsh Sinha, Jonathan T. Barron, Sofien Bouaziz, Dan B Goldman, Steven M. Seitz, and Ricardo Martin-Brualla. Nerfies: Deformable Neural Radiance Fields. *International Conference on Computer Vision (ICCV)*, 2021. 2, 3
- [29] Keunhong Park, Utkarsh Sinha, Peter Hedman, Jonathan T. Barron, Sofien Bouaziz, Dan B Goldman, Ricardo Martin-Brualla, and Steven M. Seitz. HyperNeRF: a higher-dimensional representation for topologically varying neural radiance fields. *ACM Transactions on Graphics*, 40(6), 2021. 2, 3
- [30] Albert Pumarola, Enric Corona, Gerard Pons-Moll, and Francesc Moreno-Noguer. D-NeRF: Neural Radiance Fields for Dynamic Scenes. In *Computer Vision and Pattern Recognition Conference (CVPR)*, 2021. 2, 3
- [31] Chris Rockwell, Joseph Tung, Tsung-Yi Lin, Ming-Yu Liu, David F. Fouhey, and Chen-Hsuan Lin. Dynamic Camera Poses and Where to Find Them. In *Computer Vision and Pattern Recognition Conference (CVPR)*, 2025. 3
- [32] Neus Sabater, Guillaume Boisson, Benoit Vandame, Paul Kerbiriou, Frederic Babon, et al. Dataset and Pipeline for Multi-view Light-Field Video. In *IEEE / CVF Computer Vision and Pattern Recognition Conference Workshops (CVPRW)*, 2017. 2, 3, 4
- [33] Johannes Lutz Schönberger and Jan-Michael Frahm. Structure-from-Motion Revisited. In *Computer Vision and Pattern Recognition Conference (CVPR)*, 2016. 1
- [34] Ruizhi Shao, Zerong Zheng, Hanzhang Tu, Boning Liu, Hongwen Zhang, and Yebin Liu. Tensor4D: Efficient Neural 4D Decomposition for High-fidelity Dynamic Reconstruction and Rendering. In *Computer Vision and Pattern Recognition Conference (CVPR)*, 2023. 2
- [35] Richard Shaw, Michal Nazarczuk, Jifei Song, Arthur Moreau, Sibi Catley-Chandar, Helisa Dharmo, and Eduardo Pérez-Pellitero. SWinGS: Sliding Windows for Dynamic 3D Gaussian Splatting. In *European Conference on Computer Vision (ECCV)*, 2024. 3
- [36] S. Umeyama. Least-squares estimation of transformation parameters between two point patterns. *IEEE Transactions on Pattern Analysis and Machine Intelligence*, 13(4):376–380, 1991. 8
- [37] Feng Wang, Sinan Tan, Xinghang Li, Zeyue Tian, and Huaping Liu. Mixed Neural Voxels for Fast Multi-view Video Synthesis. In *International Conference on Computer Vision (ICCV)*, 2023. 2
- [38] Jianyuan Wang, Minghao Chen, Nikita Karaev, Andrea Vedaldi, Christian Rupprecht, and David Novotny. VGGT: Visual Geometry Grounded Transformer. In *Computer Vision and Pattern Recognition Conference (CVPR)*, 2025. 1, 3, 7, 8
- [39] Shuzhe Wang, Vincent Leroy, Yohann Cabon, Boris Chidlovskii, and Jerome Revaud. Dust3r: Geometric 3d vision made easy. In *Computer Vision and Pattern Recognition Conference (CVPR)*, 2024. 3
- [40] Yifan Wang, Jianjun Zhou, Haoyi Zhu, Wenzheng Chang, Yang Zhou, Zizun Li, Junyi Chen, Jiangmiao Pang, Chunhua Shen, and Tong He. π^3 : Permutation-Equivariant Visual Geometry Learning. *arXiv preprint arXiv:2507.13347*, 2025. 3, 7, 8
- [41] Zhou Wang, A.C. Bovik, H.R. Sheikh, and E.P. Simoncelli. Image quality assessment: from error visibility to structural similarity. *IEEE TIP*, 13(4), 2004. 5
- [42] Guanjun Wu, Taoran Yi, Jiemin Fang, Lingxi Xie, Xiaopeng Zhang, Wei Wei, Wenyu Liu, Qi Tian, and Xinggang Wang. 4D Gaussian Splatting for Real-Time Dynamic Scene Rendering. In *Computer Vision and Pattern Recognition Conference (CVPR)*, 2024. 2, 5, 6
- [43] Ziyi Yang, Xinyu Gao, Wen Zhou, Shaohui Jiao, Yuqing Zhang, and Xiaogang Jin. Deformable 3D Gaussians for High-Fidelity Monocular Dynamic Scene Reconstruction. In *Computer Vision and Pattern Recognition Conference (CVPR)*, 2024. 3, 5
- [44] Jae Shin Yoon, Kihwan Kim, Orazio Gallo, Hyun Soo Park, and Jan Kautz. Novel view synthesis of dynamic scenes with globally coherent depths from a monocular camera. In *Computer Vision and Pattern Recognition Conference (CVPR)*, 2020. 2, 3
- [45] Alex Yu, Vickie Ye, Matthew Tancik, and Angjoo Kanazawa. pixelNeRF: Neural Radiance Fields from One or Few Images. In *Computer Vision and Pattern Recognition Conference (CVPR)*, 2021. 4
- [46] Richard Zhang, Phillip Isola, Alexei A Efros, Eli Shechtman, and Oliver Wang. The Unreasonable Effectiveness of Deep Features as a Perceptual Metric. In *Computer Vision and Pattern Recognition Conference (CVPR)*, 2018. 5
- [47] Shangzhan Zhang, Jianyuan Wang, Yinghao Xu, Nan Xue, Christian Rupprecht, Xiaowei Zhou, Yujun Shen, and Gordon Wetzstein. Flare: Feed-forward geometry, appearance and camera estimation from uncalibrated sparse views. In *Computer Vision and Pattern Recognition Conference (CVPR)*, 2025. 3
- [48] Ruijie Zhu, Yanzhe Liang, Hanzhi Chang, Jiacheng Deng, Jiahao Lu, Wenfei Yang, Tianzhu Zhang, and Yongdong Zhang. MotionGS: Exploring Explicit Motion Guidance for Deformable 3D Gaussian Splatting. In *Conference on Neural Information Processing Systems*, 2024. 2, 3